`

Revealing Strain Induced Effects in Ultrathin Heterostructures at the Nanoscale

Syed Ghazi Sarwat, Martin Tweedie, Benjamin F Porter, Yingqiu Zhou,Yuewen Sheng, Jan Mol, Jamie Warner, Harish Bhaskaran*

Department of Materials, University of Oxford, Oxford, OX1 3PH, UK

Two dimensional materials are being increasingly studied, particularly for flexible and wearable technologies because of their inherent thickness and flexibility. Crucially, one aspect where our understanding is still limited is on the effect of mechanical strain, not on individual sheets of materials, but when stacked together as heterostructures in devices. In this paper, we demonstrate the use of Kelvin Probe Microscopy in capturing the influence of uniaxial tensile strain on the band-structures of Graphene and WS_2 (mono and multi-layered) based heterostructures at high resolution. We report a major advance in strain characterization tools through enabling a single-shot capture of strain defined changes in a heterogeneous system at the nanoscale, overcoming the limitations (materials, resolution and substrate effects) of existing techniques such as optical spectroscopy. Using this technique we observe that the work-functions of Graphene and WS_2 increase as a function of strain, which we attribute to the Fermi level lowering from increased p-doping. We also extract the nature of the interfacial heterojunctions and find that they get strongly modulated from strain. We observe that the strain-enhanced charge transfer with the substrate plays a dominant role, causing the heterostructures to behave differently from two dimensional materials in their isolated forms.

Keywords: Two Dimensional Materials, Mechanical Strain, Kelvin Probe Microscopy, Work-Function

`

Two dimensional materials, in particular Graphene and transition metal dichalcogenides (TMDC) such as tungsten disulphide (WS_2) have made rapid progress in defining a new generation of nanoelectronics; these while pushing the performance limits of current silicon technology also extends the scaling limits to the sub-5 nanometer scale[1]. One application for which two dimensional materials are uniquely well-suited is wearable and flexible technologies, owing to their intrinsic mechanical flexibility/elasticity, and optical transparency[2]. A variety of applications, from flexible photodetectors[3], transistors[4], and photovoltaics[5] to data storage[6], gas sensors[7] and artificial skin[8], have thus far been demonstrated, mostly through combinations of various two dimensional materials. Commonly, devices are grown by chemical vapour deposition (CVD), where Graphene is used as the electrode[9,10] and TMDCs as the active units[11].

A unique characteristic of most two dimensional materials is the property of tunability, i.e., their physical and chemical properties can be tuned through varying the number of stacking layers[12], and/or by application of external stimuli, such as mechanical strain[2,13,14] and electric field[4]. The role of strain is particularly relevant in flexible and wearable technologies, where materials would always bear a certain degree of variable strain. Strain is capable of causing semiconductor-metallic[15] and direct-indirect bandgap transitions[16], bandgap change[17], Schottky barrier height shifts and/or physical debonding[13]. Whilst they can be detrimental to the device performance, they can also be harnessed for use in making field effect transistors[13,18] , strain sensors[8] and in catalysis[19]. Thus, there has been significant progress in understanding the underlying effect of strain on isolated two dimensional materials. However, real-world devices use heterostructures of these materials and techniques to study strain induced effects at the nanoscale in CVD based two dimensional heterostructures would be ideal.

In this paper, using Graphene-WS_2 heterostructure (van der Waals) on a flexible substrate (PEN- Poly ethylene naphthalene) as a demonstrator system, we illustrate an in-situ characterization technique using Kelvin Probe Microscopy (KPM) that enables characterization of strain transfer in a strain sensitive multi-component system. Using this technique we study

the effect of strain on the work function of Graphene (1-2 layered), and monolayer-multilayer (crystal) WS_2.

CVD grown multi-layer (1-2 layers) Graphene and monolayer/multi-layer WS_2 are used for the study (see Section S1). Graphene-WS_2 heterostructure are fabricated by first wet-transferring Graphene onto a PEN substrate, followed by the transfer of WS_2 (see Section S2). Optical characterization reveal graphene and WS_2 to be homogenous and of good quality (see Section S3). After transfer, the devices were annealed at 100 ^{0}C for 40 minutes in room conditions inorder to improve the adhesion of graphene and WS_2 with each other and with the substrate. We chose PEN as the substrate for its higher glass transition temperature (121 ^{0}C) which allowed for annealing at this temperature. Our set-up utilizes a custom-built sample holder and strain driver for two point bending measurements and KPM (see Figure 1A which illustrates a schematic of the setup). The atomic force microscopy (AFM) cantilevers (n-doped Si) were calibrated for their work function against highly oriented pyrolytic graphite (HOPG). The strain imparted on two dimensional materials from bending a flexible substrate on which they reside has been approximated using a continuous mechanics model for elastic beams. Based on this model, shear and normal stresses have been considered negligible since the dominant deformation occurs along the longitudinal direction. If strong coupling is assumed between PEN and the two dimensional materials, which is often the case due to strong van der Waals interaction at the interface, the strain on the two dimensional materials can be represented by the equation[16,20] $\varepsilon = \tau \times sin\theta/d$, where τ is the PEN substrate thickness (200 μm), θ is the angle between the tangent to the curved substrate and the normal to the clamp, and d is the distance between the substrate edges (see inset of Figure 1A). In our AFM set-up, the sample is grounded, and DC/AC bias is applied to the AFM cantilever.

KPM is a form of scanning probe microscopy that measures the electrostatic potential distribution over a conductive substrate[21]. This is done through measurements of the contact potential difference (CPD) between the two dimensional materials (Graphene, and WS_2), and

the AFM tip. The work function of the two dimensional materials can be derived from CPD, using the relation $\Phi_{sample}(x,y) = \Phi_{tip} - e \times CPD(x,y)$, where Φ is the work function, and e is elementary charge. Unlike photoluminescence spectroscopy, a commonly used strain characterization tool for two dimensional materials[22–24], KPM measures the changes in the work function of the materials and not their bandgaps. Therefore, as we demonstrate, KPM enables measurement of strain influence on zero-bandgap and indirect bandgap materials such as Graphene and WS_2 multilayer, respectively, and at the nanoscale. Use of KPM also overcomes any substrate effects (such as suppression and masking of material dependent signature vibrational modes), which may limit characterization of strain effects (see Figure S2). Furthermore, we find that KPM also aid the understanding of charge transport through the visualization of junction potentials.

Figure 1B is an optical micrograph of a typical sample. Individual WS_2 domains are visible, while the Graphene film on which these domains sit is indiscernible with an optical microscope (due to the high optical transparency and uniform coverage of Graphene). An example of a KPM scan of the outlined region in Figure 1B is illustrated in Figure 1C. Due to their atomic thickness, Graphene and WS_2 (including other two dimensional materials) are difficult to resolve under normal topographic AFM measurements on flexible substrates (see Figure S4 A and B), as their thickness is lesser or of the same order as the substrate‘s roughness (see Figure S4 C). KPM however, resolves them quite distinctly, thus enabling identification. Figure 1C reveals three regions of distinct electrostatic potentials. These regions correspond to Graphene (S1), monolayer WS_2 (S2) and multilayer WS_2 (S3), respectively. The smaller potential of monolayer WS_2 over multi-layer WS_2 is indicative of the thickness (number of layers) induced lowering of the work-function[12]. At zero strain, the work functions (see Figure 2A) of S1, S2 and S3 are 4.75 eV, 4.54 eV and 4.72 eV, respectively. These values agree well with literature[26–28], and are suggestive of Graphene being in a *p*-doped state, and WS_2 in an *n*-doped state. However, we note that these values can be influenced significantly by the

environment and vary between samples. For example, we observe that commonly used organic solvents can influence the work-functions of Graphene and WS_2 and this occurs at very different rates (Graphene is more readily affected than WS_2); in particular acetone results in an increased *p*-doping (see Figure S5), which is likely a result of the electron withdrawing nature of the carbonyl group in acetone. We associate the differences in the work functions between the two samples, which were fabricated with a time lag of a month (see Figure 2A and B) to the fabrication process (such as effects from solvents and sacrificial polymer) and relative humidity[29]. We note that for multi-layered WS_2, this difference is most pronounced. This is attributed to the differences in the thickness (81 layers in sample 1 and 91 layers in sample 2) and to the W:S ratio, both, within (different domains) and across the two samples (see Figure S6 and Figure S7). We find that the WS_2 domains are mostly hexagonal (irregular) rather than triangular as has been commonly reported. This follows from the understanding that shapes of individual WS_2 domains can be a strong function of their location during growth on the silicon substrate (local variations in temperature and pressure in the CVD chamber) that could result to variations in the W:S ratio, as has been previously studied in MoS_2[30,31]

We performed an independent set of standard field effect measurements (see Figure 2C) using a 300 nm SiO_2 back gate to further confirm the nature of doping predicted by KPM in Graphene and WS_2. Previous reports have confirmed that adsorbates (H_2O, O_2) and charge traps such as oxygen dangling bonds on the SiO_2 surface induce *p*-doping in two dimensional materials[25,32,33]; this behaviour, as we explain next, approximates the PEN substrate. We find that Graphene and WS_2 are indeed *p*-doped and *n*-doped, respectively. The carrier mobility is estimated using the equation $\mu = (L / WC_i V_{DS})(dI_{DS} / dV_G)$, where L and W are channel length and width, respectively, V_{DS} is the source-drain bias and C_i is the gate capacitance (11.505e-9 F/cm^2); for graphene and WS_2 the mobilities are 996 cm^2 V^{-1}s^{-1} and 0.22 cm^2 V^{-1}s^{-1}, respectively; values typical of CVD grown materials due to larger defect densities (see Figure S1) that are resultant from contamination (during growth, transfer and handling)[34,35]

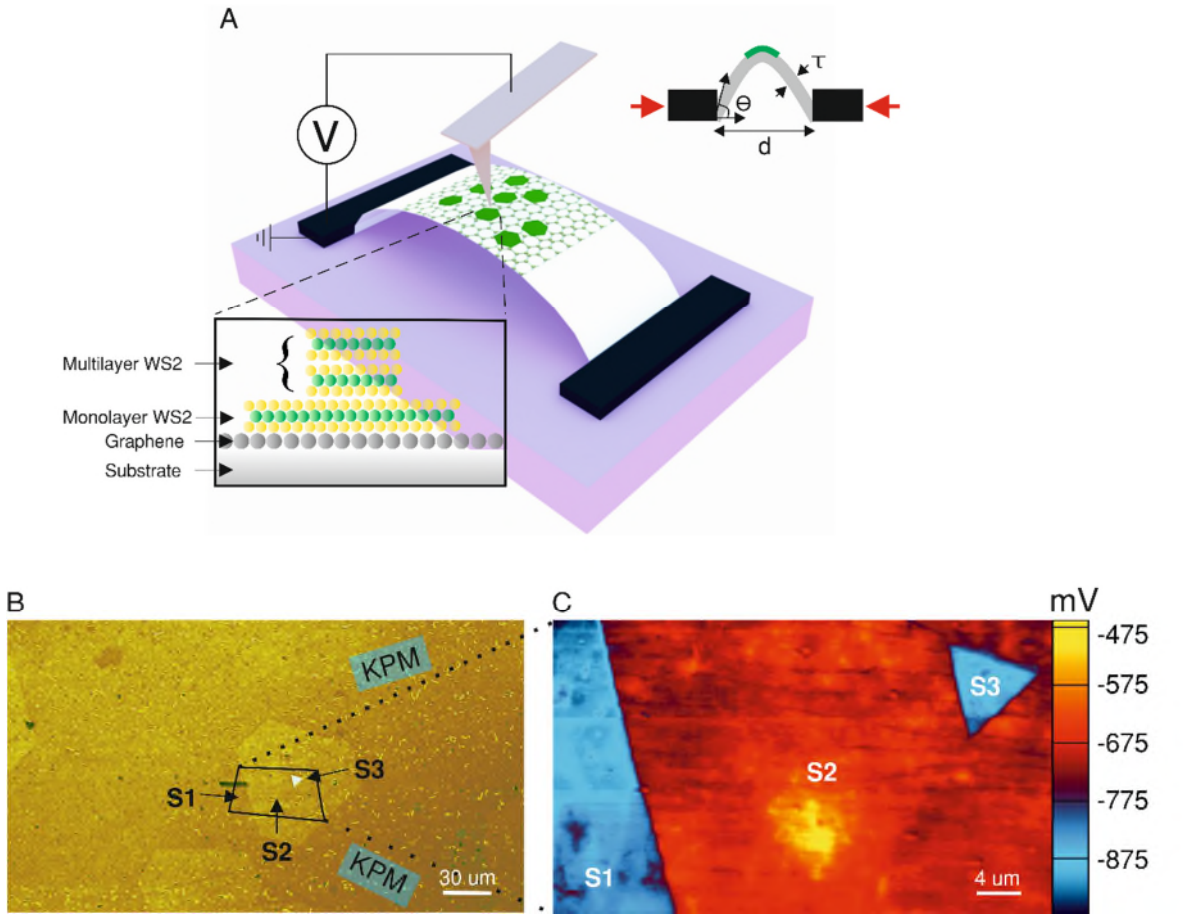

Figure 1: Two dimensional heterostructures on PEN substrate. (A) A schematic illustration of the strain characterization set-up. Top right Inset is a schematic of the two-point bending apparatus. The strain is estimated using the equation $\varepsilon = \tau \times sin\theta/d$. Bottom left inset illustrates the heterostructure consisting Graphene/WS_2 monolayer/WS_2 multilayer. B) A false coloured optical micrograph of a typical sample revealing Graphene/WS_2 heterostructure placed on a PEN substrate. S1, S2 and S3 correspond to Graphene, monolayer WS_2 and multi-layer WS_2 respectively and (C) Kelvin Probe Micrograph of the highlighted region in (B).

In order to study the effect of strain on the work functions in these regions, we applied a varying uniaxial tensile stress on the substrate through our strain driver, and recorded the work functions. We strained the devices below 1 % strain, multiple times to remove any residual stresses that may have resulted from the annealing step prior to KPM measurements. On the KPM measurements, we observe that the work function in all the three regions increases with strain (see Figure 2A and 2B). Furthermore, the fact that the change in the work function of WS_2 responds proportionally with Graphene implies an effective strain transfer between Graphene

and WS_2. This is suggestive of strong van der Waals interaction/coupling between Graphene and WS_2, which is crucial in determining their charge transfer efficiency and mechanical stability. We find that the degree of modulation in the work function per unit strain is different for Graphene and multi/mono layered WS_2. These can be calculated on first approximation using the slope of a linear fit and reach values as high as 0.117 eV for Graphene, 0.098 eV for multilayered WS_2 and 0.089 eV for monolayered WS_2. We emphasize that these are signifcant modulation in the work functions. The work functions on the reverse cycles are found to not particularly follow a trend and match the values on the forward cycles, which we attribute to the viscoelastic nature of PEN and to the fact that slipped Graphene and WS_2 adhere differently to the substrate (we discuss this later in the article). We however note the work functions of graphene and WS_2 retract to their original state each time after our cyclic measurements. In cases where graphene and WS_2 slipped, an annealing step on the hotplate at 100 ^{0}C for 10 mins could restore the original work function values for subsequent measurements. Given the response of the materials to strain being non-linear, we believe an imperfect strain transfer occurs between the substrate and the two dimensional materials. This implicity indicates that the geometrical strains do not equal the actual strain felt by graphene and WS_2, which stands contrary to assumption made in literature[20].

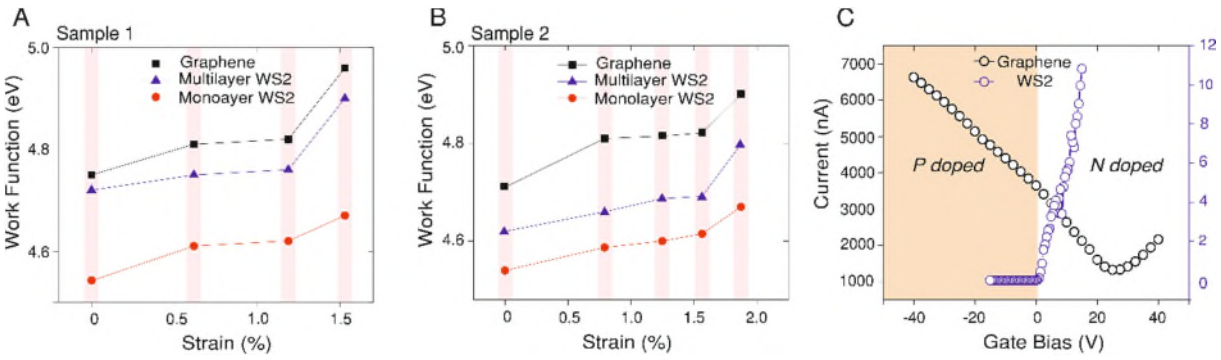

Figure 2: Strain characterization. (A and B) Plots illustrating work function of Graphene, monolayer WS_2 and multi-layer WS_2 on PEN in two different samples; the work function increases with strain. (C) Field effect (gate) measurements of Graphene and monolayer WS_2 channels on a SiO_2 substrate indicating WS_2 is n-doped, while

Graphene is *p*-doped. This measurement is difficult to perform on the PEN because of its high roughness, high defect density and large thickness.

Our observations on the strain induced increase in the work function can be attributed to the modulation of the electronic energy landscapes (energy band diagrams) of Graphene and WS_2. Such a modulation must originate from the interplay of uniaxial tensile strain and charge transfer with the PEN substrate since the changes in the work function are significant. The effect of uniaxial strain on the work function would depend on how the Fermi level and the vacuum level are modulated ($\Phi = E_{Fermi} - E_{Vaccuum}$). While for bulk materials, these effects are well understood, for two dimensional materials, particularly TMDCs, the theoretical and experimental results do not consistently support each other[2,14,36].

It is understood that in the case of M-X systems (which WS_2 is) strain can modulate the in-plane W-S bond length, while distorting the out-of-plane S-W-S in terms of both length and angle. Tensile strain theoretical calculations[14,37] suggest that in WS_2 (unlike $MoTe_2$) this results in the work function to decrease at a slower rate as the vacuum level is also modulated with strain. However, this is contradictory to our observations (we observe an increase in the work function), and also to a previous experimental study on WS_2[36]. We attribute this discrepancy to the nature of theoretical calculations, which considers WS_2 in its isolated form, ignoring the effects of substrates and environment. Charge transfer with the substrate, which depends on the degree of adhesion[38,39] and strain ehanced chemical reactivity[40,41] can also play a significant role in modulating the work function. The chemistry of PEN, which is composed of the electron-withdrawing aromatic rings and ester groups should induce *p*-doping (or decreased *n*-doping) in the two dimensional materials[42]. *P* doping implies Fermi level lowering or work function increase as correctly observed in our experiments. Using this line of reasoning, we attribute the last data point in Figure 2A and B to improved conformation of the two dimensional materials onto the substrate roughness and their enhanced chemical reactivity from strain that congruously results in improved charge transfer.

On the other hand since Graphene is formed by a single sheet of carbon atoms, all the carbon-carbon bonds get elongated under the uniaxial tensile strain. Strain induced lowering of Graphene's work function has been associated to changes in its density of states (DOS)[43]. An increase in the lattice parameter is understood to cause an increase in the DOS of Graphene due to decreased average anisotropic Fermi group velocities. Consequently, increased DOS results in the lowering of the Fermi level as higher energy electrons can fill the lower energy states. Overall, this results in an increase in the work function, as has been correctly observed in this study and in another study, where the substrate was polydimethylsiloxane (PDMS)[44]. In comparison however, we observe a relatively larger change in work function. This can be attributed to our choice of substrate, which unlike PDMS has a smaller Poisson's ratio, owing to which Graphene does not undergo significant lateral compression with uniaxial tension[22], and to enhanced *p*-doping from PEN and adsorbed molecules due to charge transfer. Therefore Graphene's Fermi level is more effectively modulated, resulting in a larger change in the work function.

We performed in situ optical spectroscopic measurements (see Figure S8) to back our KPM based observations. We find that in the case of monolayer WS_2, the E_{2g}^1 Raman peak that defines the in-plane vibrations (anti-parallel W and S vibrations) red-shifts by 2.2 cm^{-1} from strain (2%). In essence, this is indicative of lattice expansion as would be expected from a tensile strain. The A_{1g} Raman peak that defines the out-of-plane vibrations of S atoms however is suppressed due to the large back-ground noise (signal). In multi-layered WS_2 a similar strain (2%) response is observed as in monolayer; the E_{2g}^1 red-shifts by 1.77 cm^{-1} upon strain, and the A_{1g} peaks which gets evident in multi-layered WS_2 due to its greater thickness also red-shifts by 1.06 cm^{-1} with strain (2%). This anomolous A_{1g} mode softening can be although not entirely associated to doping and/or to strain and thickness induced changes in intra/inter-layer bonding[45,46]. For doping to govern this peak shift, the change has to be more significant than one observed in our case[43], and because we observe work function increase with strain, it is

more likely that the changes in the intra/inter-layer bonding is dominant in the peak shift. Infact these observations of red-shifts in the E_{2g}^1 and A_{1g} (with $E_{2g}^1 > A_{1g}$) modes are in a good agreement with a recent study on the effect of uniaxial strain on the Raman spectrum of WS_2[47]. In addition, we note from these measurements that monolayer WS_2 is modulated more strongly than the multilayer counterpart. This greater sensitivity of mono-layer WS_2 to strain over multi-layer has also been observed in multi-layered -MoS_2 and -Graphene, and -exfoliated WS_2 and is associated with the variations in the intra-layer bonding as more layers gets stacked on monolayers of these materials[47–49]. In graphene we observe that the signature Raman peaks become subtle on PEN substrate, partly due to overlapping (G) peaks and partly because of the suppression from hybridization and larger back ground noise (signal); these factors limit understanding the strain induced effects in graphene[50]. Using photoluminescence spectroscopy we find clear red-shifts in the peak position (that defines direct valence to conduction band transitions) of both mono-layered and multi-layered WS_2. This is indicative of band-gap reduction and is in agreement with previous reports on WS_2[23].

Since Graphene, WS_2 monolayers and WS_2 multilayers have different doping levels and band gaps, their Fermi levels in an uncontacted state will be different. When in contact, charge transfer occurs in order to equalise the Fermi levels, which results to the formation of junctions. We can estimate the nature of these juntions from our KPM measurements. We find that a Schottky barrier forms at the lateral Graphene/WS_2 interface, while a type-I heterojunction forms at the lateral WS_2 monolayer/WS_2 multi-layer interface. In a non-strained state, we estimate the conduction band offsets and Shocktty barrier height using the following equations

$$\Phi_{WS2multilayer} - \Phi_{WS2monolayer} = \Delta E_C - (3/2 \times KT \times ln\,(m_{mono}/m_{ulti})) \quad (1)$$

$$\Phi_{shocktty} = \Phi_{Graphene} - E_{affinity\,(WS2)} \quad (2)$$

Equation 1 makes a Boltzmann approximation, and considers identical doping levels per unit volume in monolayered and multilayered WS_2[12]. ΔE_C is the conduction band offset at the junction between mono and multilayered WS_2, K is the Boltzmann constant, T is the

temperature, and m_{mono} ($0.349m_0$) and m_{multi} ($0.569m_0$) are effective masses of electrons[51]. At zero strain, the conduction band offset between mono-layered and multilayered WS_2 in sample 1 is computed to be 181 meV. Given the band gaps of monolayered and multilayered WS_2 to be 2.14 eV and 1.4 eV, repectively[52], this indicates a type-I heterojunction. At the Graphene/mono-layer WS_2 junction, for the given electron affinity ($E_{affinity}$)[53] of 4.0 eV for WS_2, we estimate a Schottky barrier height ($\Phi_{shocktty}$) of 0.6 eV (using equation 2). This value matches with our experimental field effect measurements on SiO_2 substrate in a previous study[11]. This, while backing the accuracy of results also supports our reasoning of approximating the *p*-doping nature of SiO_2.

We however emphasize that these band offsets and the barrier height at the junctions also possess an offset due to interactions with the underlying Graphene film (this interaction is in the vertical direction and is expected to originate from the formations of dipoles rather than from Schottky barriers, owing to the atomic thicknesses of WS_2). For this discussions of our results it is sufficient that we focus on the Fermi levels of Graphene and WS_2 since both the nature and magnitude of the juntions is dependent on the differences in the Fermi levels between Graphene, monolayered and multilayered WS_2. The difference between Fermi levels of Graphene/WS_2 monolayer and WS_2 monolayer/WS_2 multi-layer can be obtained by computing the difference in their CPDs[54] ($\Delta CPD_{WS2monolayer\text{-}Graphene}$ and $\Delta CPD_{WS2monolayer\text{-}WS2multilayer}$)

$$\Delta CPD_{(WS2monolayer\text{-}Graphene/WS2multilayer)} = \Phi_{WS2multilayer} - \Phi_{Graphene/WS2monolayer} = \Delta E_{Fermi} \quad (3)$$

Figure 3A represents a typical KPM line scan at 0.6 % strain. The highlighted region marks the WS_2 monolayer/WS_2 multi-layer interface. A value ΔE_{Fermi} = 0.145 eV, and a depletion width of 2 μm can be extracted from WS_2 monolayer/WS_2 multi-layer junction (see Figure 3A). This indicates that the Fermi level of WS_2 monolayer is higher than WS_2 multilayer by 0.145 eV, suggesting a *p-n* junction at the interface. We further estimated the built-in potential and the field by fitting the junction with a sigmoidal function (see Figure 3B). The built-in potential is 0.14 eV. If we approximate WS_2 multilayer for MoS_2 monolayer (a

reasonable approximation on the basis of similar bandgaps), this value matches with the experimentally observed open circuit voltage of WS_2/MoS_2 junctions[54]. The derivative of the sigmoidal fitting is illustrated in the inset of Figure 3B and represents the electric field profile at the interface. The maximum field is at the centre of the depletion region (162 mV/μm). The effect of strain on the built-in potential, hence electric field is illustrated in Figure 3C (see Figure S9 for sample 2). We note that the built-in potential shows a non-linear behaviour with strain: a decrease is akin to applying a forward electrical bias and an increase akin to applying a reverse electrical bias. Regardless of the direction, this has significant implications as junctions govern the electrical (charge flow) and optoelectronic (photo -voltaic and -conductive) functioning of two dimensional heterostructure based devices[55].

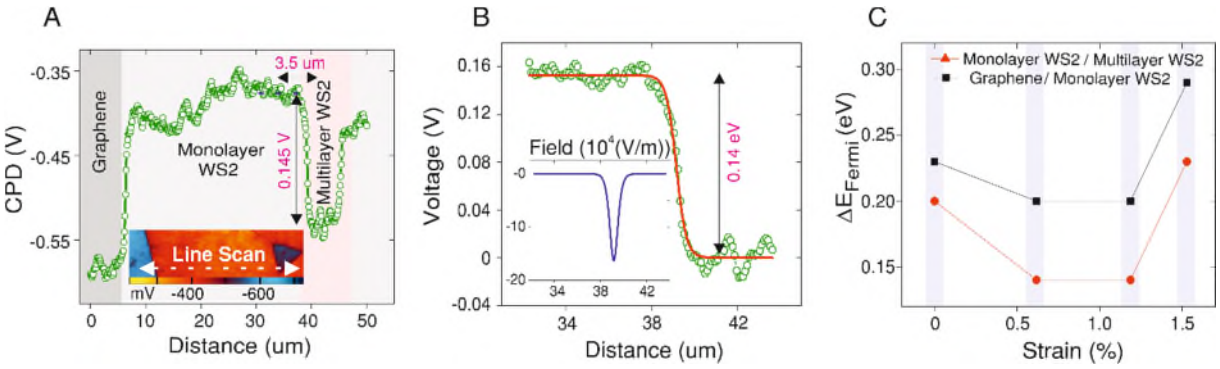

Figure 3: Heterojunctions characterization. (A) A KPM line scan on sample 1 when strained at 0.6 %. The region with arrows is the interface between monolayer WS_2 and multilayer WS_2 which behaves like a *p-n* junction with a built-in potential of 0.14 V and depletion width of 2 μm. Inset is the KPM micrograph of sample 1 at 0.6% strain. (B) The junction is fitted with a sigmodial function, and its derivative is plotted in the inset which represents the electric field profile; the direction of the field is from multi-layer WS_2 to monolayer WS_2, and (C) Plot illustrating strain modulated junctions. Strain can either increase or decrease the Schottky barrier height and built-in potentials at the Graphene/WS_2 and monolayer WS_2/multi-layer WS_2 interfaces, respectively, due to anisotropic modulation of the work functions.

We now analyze the energy band diagrams of Graphene and mono/multi-layer WS_2 under relaxed and strained conditions. In their isolated states, the Fermi levels of the Graphene, mono and multi-layer WS_2 are different and distinct with respect to each other and the AFM tip. From the KPM and gate sweep measurements, we deduce that the AFM tip and WS_2 are *n*-doped, while Graphene is *p*-doped (see Figure 4A (red dashed lines)). When the two dimensional materials are in contact with each other, an equilibrium is achieved such that a new Fermi level is established under zero strain conditions (represented by the green dashed lines in Figure 4B and 4C). The uniaxial tensile strain disturbs the equilibrium (giving rise to quasi Fermi levels). In Graphene, the Fermi level moves downwards due to increased DOS and enhanced electron transfer to PEN and adsorbed molecules from strain mediated increase in its adhesion and chemical reactivity; Graphene becomes more *p*-doped. No significant shift in the vacuum level is expected based on theoretical foundations[56]. Overall, this results in an increase in the work function. The new Fermi level of Graphene synergistically affects WS_2. In WS_2, with strain, the electrons diffuse into Graphene due to Graphene's lower Fermi level; this consequently lowering its Fermi level. Thus, decreased *n*-doping of WS_2 depends on how well Graphene gets *p*-doped. In addition, strain enhanced chemical reactivity can further *p*-dope WS_2. This is in agreement with our experimental observations: changes in the work function of WS_2 closely follows that in Graphene. However, for the work function to increase in WS_2, its vacuum level, which is theorized on first principle calculations to decrease with strain[14], has to decrease at a slower rate than the decrease in its Fermi level from charge transfer (and it does as observed experimentally in the present study). Furthermore, we note a monotonous bandgap shortening in WS_2 from the application of uniaxial tensile strain using photoluminescence spectroscopy (see Figure S10A), which complements the literature[23,45].

We also observed drops in the work functions at certain strains (see Figure S10B), which were followed by an increase. We attribute these drops to slippage or slip-driven relaxation. Slippage is a phenomenon commonly observed in two dimensional materials under unanchored

conditions[13] (as in this study), and deteriorates the adhesion between Graphene and WS_2 with the substrate resulting in an ineffective strain and charge transfer. Slip is also evident on our photoluminescence spectroscopy measurements (Figure S10A). Overall, clear signatures of strain induced changes in the electronic landscape of the heterostructures can be recorded using KPM. While our results highlight the importance of gaining better knowledge of strain induced effects in such application-oriented heterostructures, these initial findings need further investigation by research groups specializing in atomic-scale, as well as finite element modelling to verify the nature of band-alignment and strain transfer.

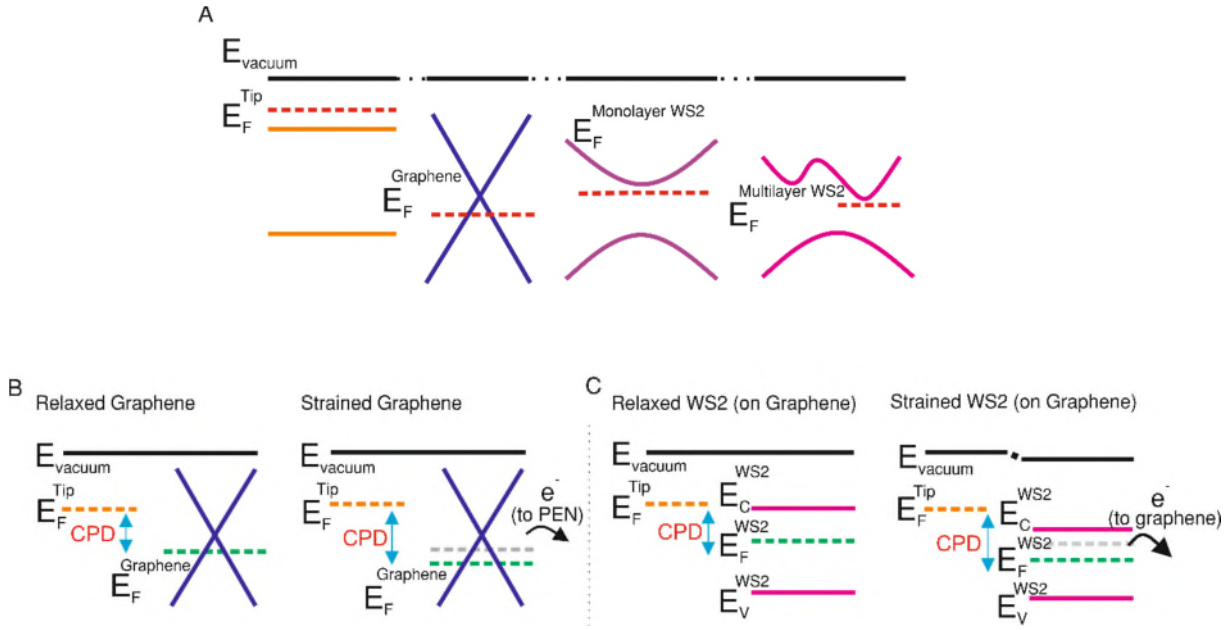

Figure 4. Energy band diagrams. (A) Electronic energy landscapes of AFM tip, Graphene, monolayer WS_2 and multi-layer WS_2 under equilibrium and isolated conditions. AFM tip and Graphene in *p*-type doped, while WS_2 is *n*-type doped (red dashed lines are the Fermi levels). At zero strain we estimate a Schokkty barrier height of 0.6 eV at Graphene/monlayered WS_2 junction, and a conduction band offset of 181 meV between monlayered/multilayered WS_2. (B and C) Uniaxial tensile strain influenced energy band diagrams of the Graphene/WS_2 heterostructure. The green dashed line represents the equilibrium Fermi level. (B) Uniaxial tensile strain downshifts the Fermi level of Graphene (E_F), illustrated by the increase in the contact potential difference (CPD). (C) Uniaxial tensile strain downshifts the Fermi level (E_F) of WS_2 (mono and multi- layer), as well as decreases the vacuum level (E_{vacuum}) and shortens the bandgaps. The decrease in the Fermi levels of Graphene and WS_2 is attributed to strain induced effects and charge transfer.

In conclusion, we have demonstrated an in-situ characterisation technique based on KPM for studying the underlying effects of varying uniaxial tensile strain in Graphene/WS_2 heterostructures. We report pronounced changes in the work functions of Graphene, mono and multi-layer WS_2, and their junctions. We note that WS_2 in heterostructure configurations behave differently to how they would in isolation. Our findings are important for both device engineering, as well as for the studies of two dimensional heterostructures. We emphasize that the use of KPM is not just limited to two dimensional materials, but to any study that requires realization of strain modulation in individual components with a nanoscale resolution in a multicomponent system and in the study of spatial strain distribution in a homogenous system.

Acknowledgements

S.G.S acknowledges a Felix Scholarship that supports his DPhil. JM acknowledges an RAEng Fellowship. G.S and H.B acknowledge support from EPSRC via the Manufacturing Fellowship EP/J018694/1 as well as the WAFT collaboration (EP/M015173/1). JHW thanks the support from the Royal Society and the European Research Council. YZ acknowledges the support from the China Scholarship Council. S.G.S acknowledges Nathan Youngblood (Dept. of Materials, University of Oxford) for proof reading the manuscript.

Supporting Information

Materials Synthesis, Device Fabrication, Optical Characterization, Work Function Extraction Methodology, Substrate Roughness, Effect of Organic Solvents, Scanning Electron Micrographs and Energy Dispersive X Ray spectroscopy data, Photoluminescence spectroscopy data, Slippage observation using KPM measurements

Authors Information

***Corresponding Author**

harish.bhaskaran@materials.ox.ac.uk

Notes

The authors declare no competing financial interests

References:

(1) Desai, S. B.; Madhvapathy, S. R.; Sachid, A. B.; Llinas, J. P.; Wang, Q.; Ahn, G. H.; Pitner, G.; Kim, M. J.; Bokor, J.; Hu, C.; *et al.* MoS_2 Transistors with 1-Nanometer Gate Lengths. **2016**, *354*, 99–103.

(2) Wurstbauer, U.; Miller, B.; Parzinger, E.; Lin, Z.; Mccreary, A.; Briggs, N.; Castellanos-gomez, A.; Vicarelli, L.; Prada, E. Strain Engineering in Semiconducting Two-Dimensional Crystals. *J. Phys. Condens. Matter* **2015**, *27*, 1–18.

(3) Fazio, D. De; Goykhman, I.; Yoon, D.; Bruna, M.; Eiden, A.; Milana, S.; Sassi, U.; Barbone, M.; Dumcenco, D.; Marinov, K.; *et al.* High Responsivity, Large-Area Graphene/MoS_2 Flexible Photodetectors. *ACS Nano* **2016**, *10*, 8252−8262.

(4) Georgiou, T.; Jalil, R.; Belle, B. D.; Britnell, L.; Gorbachev, R. V; Morozov, S. V; Kim, Y.; Gholinia, A.; Haigh, S. J.; Makarovsky, O.; *et al.* Vertical Field-Effect Transistor Based on Graphene–WS_2 Heterostructures for Flexible and Transparent Electronics. *Nat. Nanotechnol.* **2012**, *8*, 100–103.

(5) Shanmugam, M.; Jacobs-Gedrim, R.; Song, E. S.; Yu, B. Two-Dimensional Layered Semiconductor/graphene Heterostructures for Solar Photovoltaic Applications. *Nanoscale* **2014**, *6*, 12682–12689.

(6) Bertolazzi, S.; Krasnozhon, D.; Kis, A. Nonvolatile Memory Cells Based on MoS_2/Graphene. *ACS Nano* **2013**, *7*, 3246–3252.

(7) Yang, W.; GAN, L.; Li, H.; Zhai, T. Two-Dimensional Layered Nanomaterials for Gas-Sensing Applications. *Inorg. Chem. Front.* **2016**, *3*, 433–451.

(8) Feng, W.; Zheng, W.; Gao, F.; Chen, X.; Liu, G.; Hasan, T.; Cao, W.; Hu, P. Sensitive Electronic-Skin Strain Sensor Array Based on the Patterned Two-Dimensional a-In_2Se_3. *Chem. Mater.* **2016**, *28*, 4278–4283.

(9) Sarwat, S. G. Materials Science and Engineering of Phase Change Random Access Memory. *Mater. Sci. Technol.* **2017**, *836*, 1–17.

(10) Sarwat, S. G.; Gehring, P.; Rodriguez Hernandez, G.; Warner, J. H.; Briggs, G. A. D.; Mol, J. A.; Bhaskaran, H. Scaling Limits of Graphene Nanoelectrodes. *Nano Lett.* **2017**, *17*, 3688–3693.

(11) Tan, H.; Fan, Y.; Zhou, Y.; Chen, Q.; Xu, W.; Warner, J. H. Ultrathin 2D Photodetectors Utilizing Chemical Vapor Deposition Grown WS2 with Graphene Electrodes. *ACS Nano* **2016**, *10*, 7866–7873.

(12) Tosun, M.; Fu, D.; Desai, S. B.; Ko, C.; Kang, J. S.; Lien, D.; Najmzadeh, M.; Tongay, S.; Wu, J. MoS_2 Heterojunctions by Thickness Modulation. *Sci. Rep.* **2015**, *5*, 1–8.

(13) Shen, T.; Penumatcha, A. V; Appenzeller, J. Strain Engineering for Transition Metal Dichalcogenides Field Effect Transistors. *ACS Nano* **2016**, *10*, 4712–4718.

(14) Lanzillo, N. A.; Simbeck, A. J.; Nayak, S. K. Strain Engineering the Work Function in Monolayer Metal Dichalcogenides. *J. Phys. Condens. Matter* **2015**, *27*, 175501.

(15) Garg, R.; Dutta, N. K.; Choudhury, N. R. Work Function Engineering of Graphene. *Nanomaterials* **2014**, *4*, 267–300.

(16) Desai, S. B.; Seol, G.; Kang, J. S.; Fang, H.; Battaglia, C. Strain-Induced Indirect to Direct Bandgap Transition in Multilayer. *Nano Lett.* **2014**, *14*, 4592–4597.

(17) Conley, H. J.; Wang, B.; Ziegler, J. I.; Haglund, R. F.; Pantelides, S. T.; Bolotin, K. I. Bandgap Engineering of Strained Monolayer and Bilayer MoS_2. *Nano Lett.* **2013**, *13*, 3626–3630.

(18) Das, S.; Gulotty, R.; Sumant, A. V; Roelofs, A. All 2D , Flexible , Transparent and Thinnest Thin Film Transistor. *Nano Lett.* **2014**, *2*, 4–6.

(19) Bissett, M. A.; Konabe, S.; Okada, S.; Tsuji, M.; Ago, H. Enhanced Chemical Reactivity of Graphene Induced by Mechanical Strain. *ACS Nano* **2013**, *7*, 10335–10343.

(20) Roldán, R.; Castellanos-Gomez, A.; Cappelluti, E.; Guinea, F. Strain Engineering in Semiconducting Two-Dimensional Crystals. *J. Phys. Condens. Matter* **2015**, *27*, 313201.

(21) Muñoz-Rojo, M.; Caballero-Calero, O.; Martín-González, M. Electrical Contact Resistances of Thermoelectric Thin Films Measured by Kelvin Probe Microscopy. *Appl. Phys. Lett.* **2013**, *103*, 183905.

(22) Bissett, M. A.; Izumida, W.; Saito, R.; Ago, H. Effect of Domain Boundaries on the Raman Spectra of Mechanically Strained Graphene. *ACS Nano* **2012**, *6*, 10229–10238.

(23) He, X.; Li, H.; Zhu, Z.; Dai, Z.; Yang, Y.; Yang, P.; Zhang, Q.; Li, P.; Schwingenschlogl, U.; Zhang, X. Strain Engineering in Monolayer WS_2, MoS_2, and the WS_2/MoS_2 Heterostructure. *Appl. Phys. Lett.* **2016**, *109*, 173105.

(24) McCreary, A.; Ghosh, R.; Amani, M.; Wang, J.; Duerloo, K. A. N.; Sharma, A.; Jarvis, K.; Reed, E. J.; Dongare, A. M.; Banerjee, S. K.; *et al.* Effects of Uniaxial and Biaxial Strain on Few-Layered Terrace Structures of MoS_2 Grown by Vapor Transport. *ACS Nano* **2016**, *10*, 3186–3197.

(25) Nistor, R. A.; Kuroda, M. A.; Maarouf, A. A.; Martyna, G. J. Doping of Adsorbed Graphene from Defects and Impurities in SiO_2 Substrates. *Phys. Rev. B* **2012**, *41409*, 1–5.

(26) Yu, Y.-J.; Zhao, Y.; Ryu, S.; Brus, L. E.; Kim, K. S.; Kim, P. Tuning the Graphene Work Function by Electric Field Effect. Supplementary Information. *Nano Lett.* **2009**, *9*, 3430–3434.

(27) Hill, H. M.; Rigosi, A. F.; Rim, K. T.; Flynn, G. W.; Heinz, T. F. Band Alignment in MoS_2/WS_2 Transition Metal Dichalcogenide Heterostructures Probed by Scanning Tunneling Microscopy and Spectroscopy. *Nano Lett.* **2016**, *16*, 4831–4837.

(28) Kapatel, S.; Sumesh, C. K.; Pataniya, P.; Solanki, G. K.; Patel, K. D. Layer-Engineered I-V Characteristics of P-Si /WS_2 Van Der Waals Heterostructure Diode. *Eur. Phys. J. Plus* **2017**, *132*, 191.

(29) Lee, S. Y.; Kim, U. J.; Chung, J.; Nam, H.; Jeong, H. Y.; Han, G. H.; Kim, H.; Oh, H. M.; Lee, H.; Kim, H.; *et al.* Large Work Function Modulation of Monolayer MoS_2 by Ambient Gases. *ACS Nano* **2016**, *10*, 6100–6107.

(30) Xu, W.; Li, S.; Zhou, S.; Lee, J. K.; Wang, S.; Sarwat, S. G.; Wang, X.; Bhaskaran, H.; Pasta, M.; Warner, J. H. Large Dendritic Monolayer MoS 2 Grown by Atmospheric Pressure Chemical Vapor Deposition for Electrocatalysis. *ACS Appl. Mater. Interfaces* **2018**, *10*, 4630–4639.

(31) Wang, S.; Rong, Y.; Fan, Y.; Pacios, M.; Bhaskaran, H.; He, K.; Warner, J. H. Shape Evolution of Monolayer MoS_2 Crystals Grown by Chemical Vapor Deposition. *Chem. Mater.* **2014**, *26*, 6371–6379.

(32) Meng, J.; Song, H.-D.; Li, C.-Z.; Jin, Y.; Tang, L.; Liu, D.; Liao, Z.-M.; Xiu, F.; Yu, D. Lateral Graphene P–n Junctions Formed by the graphene/MoS2 Hybrid Interface. *Nanoscale* **2015**, *7*, 11611–11619.

(33) Piazza, A.; Giannazzo, F.; Buscarino, G.; Fisichella, G.; Magna, A. La; Roccaforte, F.; Cannas, M.; Gelardi, F. M.; Agnello, S. Effect of Air on Oxygen P-Doped Graphene on SiO 2. *Phys. Status Solidi A 213*, **2016**, *2344*, 2341–2344.

(34) Ahn, J.-H.; Parkin, W. M.; Naylor, C. H.; Johnson, A. T. C.; Drndić, M. Ambient Effects on Electrical Characteristics of CVD-Grown Monolayer MoS_2 Field-Effect

Transistors. *Sci. Rep.* **2017**, *7*, 4075.

(35) Song, H. S.; Li, S. L.; Miyazaki, H.; Sato, S.; Hayashi, K.; Yamada, A.; Yokoyama, N.; Tsukagoshi, K. Origin of the Relatively Low Transport Mobility of Graphene Grown through Chemical Vapor Deposition. *Sci. Rep.* **2012**, *2*, 1–6.

(36) Meng, L.; Zhang, Y.; Hu, S.; Wang, X.; Liu, C.; Guo, Y.; Wang, X. Two Dimensional WS_2 Lateral Heterojunctions by Strain Modulation Two Dimensional WS_2 Lateral Heterojunctions by Strain Modulation. *Appl. Phys. Lett.* **2016**, *263104*.

(37) Yu, L.; Ruzsinszky, A.; Perdew, J. P. Bending Two-Dimensional Materials to Control Charge Localization and Fermi-Level Shift. *Nano Lett.* **2016**, *16*, 2444–2449.

(38) Ashraf, A.; Wu, Y.; Wang, M. C.; Yong, K.; Sun, T.; Jing, Y.; Haasch, R. T.; Aluru, N. R.; Nam, S. Doping-Induced Tunable Wettability and Adhesion of Graphene. *Nano Lett.* **2016**, *16*, 4708–4712.

(39) Jung, D. Y.; Yang, S. Y.; Park, H.; Shin, W. C.; Oh, J. G.; Cho, B. J.; Choi, S.-Y. Interface Engineering for High Performance Graphene Electronic Devices. *Nano Converg.* **2015**, *2*, 11.

(40) Kou, L.; Du, A.; Chen, C.; Frauenheim, T. Strain Engineering of Selective Chemical Adsorption on Monolayer MoS_2. *Nanoscale* **2014**, *6*, 5156–5161.

(41) Bissett, M. A.; Konabe, S.; Okada, S.; Tsuji, M.; Ago, H. Enhanced Chemical Reactivity of Graphene Induced by Mechanical Strain. *ACS Nano* **2013**, *7*, 10335–10343.

(42) Dong, X.; Fu, D.; Fang, W.; Shi, Y.; Chen, P.; Li, L. Doping Single-Layer Graphene with Aromatic Molecules **. *Small* **2009**, 1422–1426.

(43) Choi, S.; Jhi, S.; Son, Y. Effects of Strain on Electronic Properties of Graphene. *Phys.*

Rev. Lett. B **2010**, *81*, 23–26.

(44) He, X.; Tang, N.; Sun, X.; Gan, L.; Ke, F.; Wang, T.; Xu, F.; Wang, X.; Yang, X.; Shen, B. Tuning the Graphene Work Function by Uniaxial Strain. *Appl. Phys. Lett.* **2015**, *43106*.

(45) Castellanos-Gomez, A.; Roldán, R.; Cappelluti, E.; Buscema, M.; Guinea, F.; Van Der Zant, H. S. J.; Steele, G. A. Local Strain Engineering in Atomically Thin MoS2. *Nano Lett.* **2013**, *13*, 5361–5366.

(46) Cho, B.; Hahm, M. G.; Choi, M.; Yoon, J.; Kim, A. R.; Lee, Y. J.; Park, S. G.; Kwon, J. D.; Kim, C. S.; Song, M.; *et al.* Charge-Transfer-Based Gas Sensing Using Atomic-Layer MoS2. *Sci. Rep.* **2015**, *5*, 8052.

(47) Wurstbauer, U.; Miller, B.; Parzinger, E.; Lin, Z.; Carvalho, B. R.; Kahn, E.; Brien, M. O.; Mcevoy, N.; Motta, C.; Wang, F.; *et al.* Strain-Induced Phonon Shifts in Tungsten Disul Fi de Nanoplatelets and Nanotubes. *2D Mater.* **2016**, *4*, 15007.

(48) Rice, C.; Young, R. J.; Zan, R.; Bangert, U.; Wolverson, D.; Georgiou, T.; Jalil, R.; Novoselov, K. S. Raman-Scattering Measurements and First-Principles Calculations of Strain-Induced Phonon Shifts in Monolayer MoS2. *Phys. Rev. B - Condens. Matter Mater. Phys.* **2013**, *87*, 1–5.

(49) Gong, L.; Young, R. J.; Kinloch, I. A.; Riaz, I.; Jalil, R.; Novoselov, K. S. Optimizing the Reinforcement of Polymer-Based Nanocomposites by Graphene. *ACS Nano* **2012**, *6*, 2086–2095.

(50) Li, Z.; Kinloch, I. A.; Young, R. J.; Novoselov, K. S.; Anagnostopoulos, G.; Parthenios, J.; Galiotis, C.; Papagelis, K.; Lu, C. Y.; Britnell, L. Deformation of Wrinkled Graphene. *ACS Nano* **2015**, *9*, 3917–3925.

(51) Reviewed, P.; Riverside, M. E. UC Riverside Electronic Theses and Dissertations. *Thesis-Electronic, Vib. Thermoelectr. Prop. Two-Dimensional Mater.* **2009**.

(52) Jo, S.; Ubrig, N.; Berger, H.; Kuzmenko, A. B.; Morpurgo, A. F. Mono- and Bilayer WS_2 Light-Emitting Transistors. *Nano Lett.* **2014**, *14*, 2019–2025.

(53) Yamaguchi, T.; Moriya, R.; Inoue, Y.; Morikawa, S. Tunneling Transport in a Few Monolayer-Thick WS_2/Graphene Heterojunction. *Appl. Phys. Lett.* **2014**, *105*, 223109.

(54) Chen, K.; Wan, X.; Xie, W.; Wen, J.; Kang, Z.; Zeng, X.; Chen, H.; Xu, J. Lateral Built-In Potential of Monolayer MoS_2–WS_2 In-Plane Heterostructures by a Shortcut Growth Strategy. *Adv. Mater.* **2015**, 6431–6437.

(55) Zheng, L.; Zhongzhu, L.; Guozhen, S. Photodetectors Based on Two Dimensional Materials. *J. Semicond.* **2016**, *37*, 1–11.

(56) Peng, X.; Tang, F.; Copple, A. Engineering the Work Function of Armchair Graphene Nanoribbons Using Strain and Functional Species: A First Principles Study. *J. Phys. Condens. Matter* **2012**, *24*, 75501.

Artwork-